SCIENTIFIC REPORTS

Tuning inter-dot tunnel coupling of an etched graphene double quantum dot by adjacent metal gates

Da Wei[1], Hai-Ou Li[1], Gang Cao[1], Gang Luo[1], Zhi-Xiong Zheng[1], Tao Tu[1], Ming Xiao[1], Guang-Can Guo[1], Hong-Wen Jiang[2] & Guo-Ping Guo[1]

[1]Key Laboratory of Quantum Information, Department of Optics and Optical Engineering, University of Science and Technology of China, Chinese Academy of Science, Hefei 230026, China, [2]Department of Physics and Astronomy, University of California at Los Angeles, California 90095, USA.

Graphene double quantum dots (DQDs) open to use charge or spin degrees of freedom for storing and manipulating quantum information in this new electronic material. However, impurities and edge disorders in etched graphene nano-structures hinder the ability to control the inter-dot tunnel coupling, t_C, the most important property of the artificial molecule. Here we report measurements of t_C in an all-metal-side-gated graphene DQD. We find that t_C can be controlled continuously about a factor of four by employing a single gate. Furthermore, t_C, can be changed monotonically about another factor of four as electrons are gate-pumped into the dot one by one. The results suggest that the strength of tunnel coupling in etched graphene DQDs can be varied in a rather broad range and in a controllable manner, which improves the outlook to use graphene as a base material for qubit applications.

Graphene, a newly discovered material which is fabricated from a few layers of its bulky origin, graphite, has attracted much recent attention for its promising variety of nano-electronics applications. Among these novel applications, several proposals have been made to store and manipulate quantum information in graphene based quantum dots, attracted by its possible long coherence time, unique band structures, and ability to oppose localization etc[1,2].

For quantum dot based quantum information processing, double quantum dots (DQDs), sometimes called artificial molecules, emerge as one of the leading candidates for qubit implementation, which can be encoded either by the bonding and anti-bonding states of charges or by the singlet and triplet states of spins. In order to perform logic operations in a DQD, for either charge qubits or spin qubits, it is essential to measure and to gain control over the tunnel coupling between two adjacent dots. This tunneling coupling is also fundamentally important for two-qubit operations. Indeed, such control has been demonstrated in DQDs made of more conventional semiconducting materials, such as GaAs/AlGaAs[3] and Si/SiGe[4]. So far graphene DQD have already been successfully fabricated by a number of groups[5–9] and the gigahertz-ranged charge pumping is also demonstrated[9]. Although in an earlier transport measurement of a more conventional graphene DQD[6], t_C was qualitatively estimated from the curvature of honeycomb edge patterns, suggesting the inter-dot coupling can be very strong, controllable inter-dot tunneling coupling in etched graphene DQDs remains to be a challenge. Such challenge may derive from the fact that the etched graphene DQD system suffers from unpredictable and usually non-monotonic changes in its inter-dot configuration. When one tries to tune the system by adjusting the local electrostatic potential, mainly due to impurities and edge states' capturing/releasing electrons, such reconfiguration happens and results in non-monotonic changes in inter-dot capacitances[10–13]. The difficulty of experimentally controlling tunneling barriers in graphene has commonly led to an intuitive worry that t_C coupling is totally uncontrollable by gate.

Here, we demonstrate that our experimental studies may suggest otherwise that etched graphene can be sufficiently controllable over an extended range of experimental parameters so they might be suitable to be used for exploratory studies of coherent quantum properties of graphene quantum dots.

In our all-metal-side-gated graphene DQD, the actual electron temperature (T_e) under base temperature and capacitances that form the charge network are accurately determined by using a refined measurement method. As a consequence, both capacitive coupling of the DQD and the inter-dot tunneling coupling can be accurately

measured. Our results show that the inter-dot tunnel coupling strength t_C strength can be tuned about a factor of 4 simply by tuning the inter-dot potential barrier through gates. Such tunability appears to be exponentially monotonic as expected for a tunneling barrier defined DQD system. In addition, we also find the relative electron number in one dot can be varied to change t_C by another factor of 4, as one adds electrons into one quantum dot one by one. Such tendencies appear to be monotonic over as many as nine consecutive electrons. In other identical sample investigated, the average monotonic tendency length is 5 electrons. Though suffering from long-range uncontrollable behaviors as reported, its tunability is sufficient for further exploratory experiments.

Based on our experimental findings, we suggest that etched graphene DQD systems may still be a suitable platform for fundamental researches in this material aiming at proof-of-principle demonstration of coherent properties of charge/spin. Especially the rapid progress in nanotechnology is expected to gain more and more control over the disorders in graphene ribbon structures, graphene DQDs may eventually become a viable candidate for solid-state qubits.

Results

Electrostatic-gate controlled graphene double quantum dots. The device used for the experiment is a double quantum dot with an integrated charge state sensor. The base graphene structures of the DQD along with the adjacent detection channel are defined by plasma etching of a large flake. The electrostatic control is facilitated by incorporating additional metallic gates, as shown in the SEM picture, in Fig. 1a. We have studied over ten identical devices. For consistency, the bulk of the data presented in this paper is from one sample.

Conventionally, the terminals of controlling gates for QDs are also formed by graphene ribbon structures[6–13]. As experiments have shown that small graphene ribbon structure (i.e., smaller than 100 nm) cannot be considered as a good conductor, as localized states are likely populated over the ribbon, we argue nano-ribbon an undesirable candidate for stable gating. Therefore to minimize the non-monotonic or sudden change in the electrostatic environment, in our device all controlling gates are made out of high-conductance

metal using precision alignment for placing them in the close proximity, as close as 40 nm, of the etched graphene ribbon structures.

As shown in Fig. 1a, the sample consists of a double-dot structure accompanied by a Quantum Point Contact (QPC) read-out channel down under. The QPC channel serves as a non-invasive detector of the charge states in the DQD system. Each dot has roughly a physical dimension of 120 nm by 80 nm, the connecting ribbon structure is of 100 nm length and 35 nm width. Specifically, the gates LP (RP) and LB (RB) are designed to control the electrochemical potential of the left dot (right dot) and left barrier (right barrier) respectively. Middle gate (marked as MG) is primarily used to tune the capacitive and the tunneling coupling of the two adjacent dots and gate Q is for the adjustment of the QPC's working point for optimum sensitivity.

Determination of electron temperature of the device. The experiment is carried out in an Oxford Instruments top-loading dilution refrigerator. The sample is in direct thermal contact with the He3/He4 liquid mixture. The base temperature of the bath is 35 mK and the bath temperature can be accurately varied from base to 700 mK.

Sweeping LP and RP at the same time we observed the characteristic signature of the formation of the DQD, known as the honeycomb diagram, as displayed for a typical sample in Fig. 1b. The charge stability diagram shows rather ordered structures for extended range of gate voltages. From such diagram we may extract nearly all the capacitances that form the charge network. Within each honeycomb, electron number for each dot is a well-defined integer. Thus, the combs are marked by $(M + j, N + i)$ to denote the relative electron numbers in left and right dots, respectively.

Such diagrams are obtained through QPC serving as an electrostatic detector. It is possible to detect all the charge transition boundaries because the conductance of QPC channel depends sensitively on the electrochemical potential of the coupled DQD systems. For DQDs in Coulomb blockade regime, the electrons are only allowed to enter the dot one by one. The discreteness in charge brings a set of discrete electrochemical energy levels in each dot. Thus, entrance of an electron in one dot will cause a sudden change in QPC conductance.
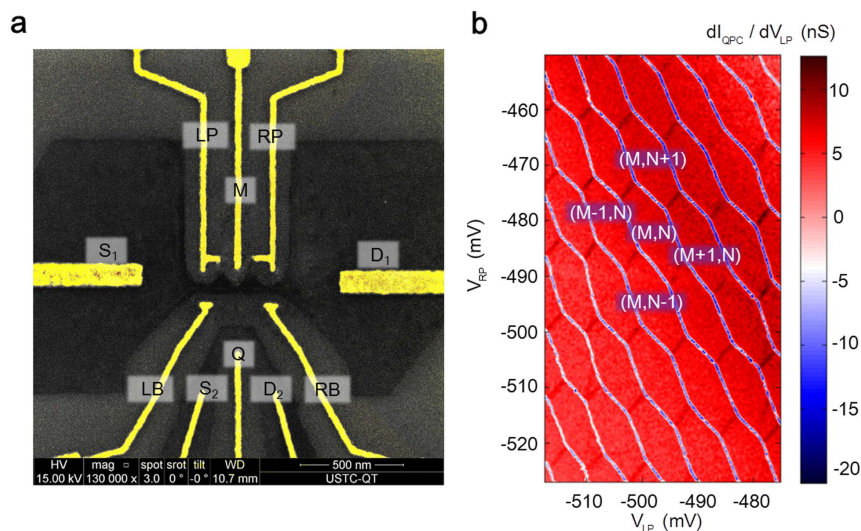

a

b

Figure 1 | Sample characterizaion. (a). Scanning electron micrograph in false color of the device. Dark regions are the graphene base structure consisting of a double quantum dot (100 nm*100 nm for each dot, 35 nm*100 nm for each ribbon) and an integrated QPC channel serving as in situ charge detector. Grey area is the etched-away region that shows the SiO_2 substrate surface. The yellow regions are the metal gates used for control and as source/drain electrodes. (b). A typical QPC charge sensor stability diagram of the double quantum dot: differential charge sensor current dI_{QPC}/dV_{LP} as a function of two gate voltages V_{LP} and V_{RP}. The structure shows a well-defined double quantum dot with characteristic honeycomb patterns. Charge state is defined by (M, N), where M and N are the electron number in the left and right dot, respectively (The charging energy and regularity are the same throughout the samples tested. The difference in the honeycomb size between Fig. 1b and the else in the article stems from doped and undoped sample substrates).

As the QPC signal is an ensemble-averaged response to the DQD system, thermal fluctuation and quantum processes such as tunneling will smear the sharpness in the conductance shift. DiCarlo et al.[3] is the first to employ the sharpness of the conductance change as a function of the detuning, for an inter-dot transition, to investigate the effective electron temperature and the tunneling coupling strength of two adjacent dots. In our measurement, we refine their technique by using a modulation technique. A small modulation voltage is superimposed onto the DC scanning voltage on RP. The signal, detected by a lock-in amplifier, is the physical derivative of the original one, known as transconductance, dI/dV_{RP}, as the transconductance signal appears to have far better signal-noise ratio than the origin conductance signal. It turns out, for our graphene devices, due to the relatively large noise background, this refinement is very much necessary in order to reliably extract the temperature and the tunneling information.

As a consequence of charge transfer from one dot to another, the transconductance gives rise to a peak. The Full Width at Half Maximum (FWHM) in unit of detuning energy of such transition peak, denoted as FWHM (eV), directly reflects the sharpness of the corresponding conductance shift. The relation between FWHM (eV), T_e and t_C is:

$$\frac{\Delta^2}{\sqrt{\Delta^2+F^2}^3}\,\text{th}\left(\sqrt{\Delta^2+F^2}\right)+\frac{F^2}{\Delta^2+F^2}\,\text{ch}^{-2}\left(\sqrt{\Delta^2+F^2}\right)=\frac{\text{th}\Delta}{2\Delta};$$

$$F=\frac{\text{FWHM(eV)}}{2}\cdot\frac{1}{2k_BT_e};\qquad(1)$$

$$\Delta=\frac{t_C}{2k_BT_e}.$$

(Eq. (1) and eq. (2) derive from two well-examined model. A detailed deduction will be given in supplementary material attached) From this expression, it is clear that the FWHM is a combination of the two intertwining parameters of T_e and t_C. It is therefore of critical importance to determine the electron temperature, which can be significantly different from the bath temperature, before a reliable t_C value can be measured.

To determine T_e we strategically select a place where t_C is very small (i.e., $t_C \ll 2k_BT_e$). In this limit, the peak width of the transition line is then directly proportional to T_e. By Setting t_C in eq.(1) to zero, one obtains the relation:

$$\text{FWHM(eV)}=2\cdot\ln\left(\sqrt{2}+1\right)\cdot2k_BT_e\approx3.5k_BT_e\qquad(2)$$

According to eq.(2), we investigate the evolution of peak width against raising mixing chamber temperature. Fig. 2 is obtained in the region where we find the tunneling strength weak enough to be neglected. We measure the peak width along the detuning line (white dashed line) as shown in Fig. 2a. Fig. 2b shows an example of this peak broadening for three mixing chamber temperatures. The results in Fig. 2c clearly display a linear dependence of FWHM on the mixing chamber temperature when temperature is high enough to provide a strong enough electron-phonon coupling so that electron is in equilibrium with the graphene lattice. From Fig. 2c, we extract the lever arm of the left plunger gate, $C_{gL}/C_L = 0.039$. Taking into consideration that the t_C of this measured transition line is no larger than 2 μeV (0.5 GHz), which is estimated through the intercept of the dashed line in Fig. 2c, we finally calculate T_e under dilution refrigerator's base temperature to be 75.3 ± 9.4 mK. This T_e is verified for several transition lines, all in the weak-coupling region.

Measurement and tunability of the inter-dot tunnel coupling strength. Once T_e is obtained, we are now capable of measuring the t_C coupling strength throughout the entire V_{LP}-V_{RP} plane. For any particular transition line, we sweep V_{LP} and V_{RP} along the detuning line, as shown before, and obtain its peak width projected in either V_{LP} or V_{RP} axis. Take V_{LP} for instance, the measured FWHM in unit of voltage, FWHM (V), is firstly converted into unit of detuning, FWHM (eV), then non-dimensionalized using
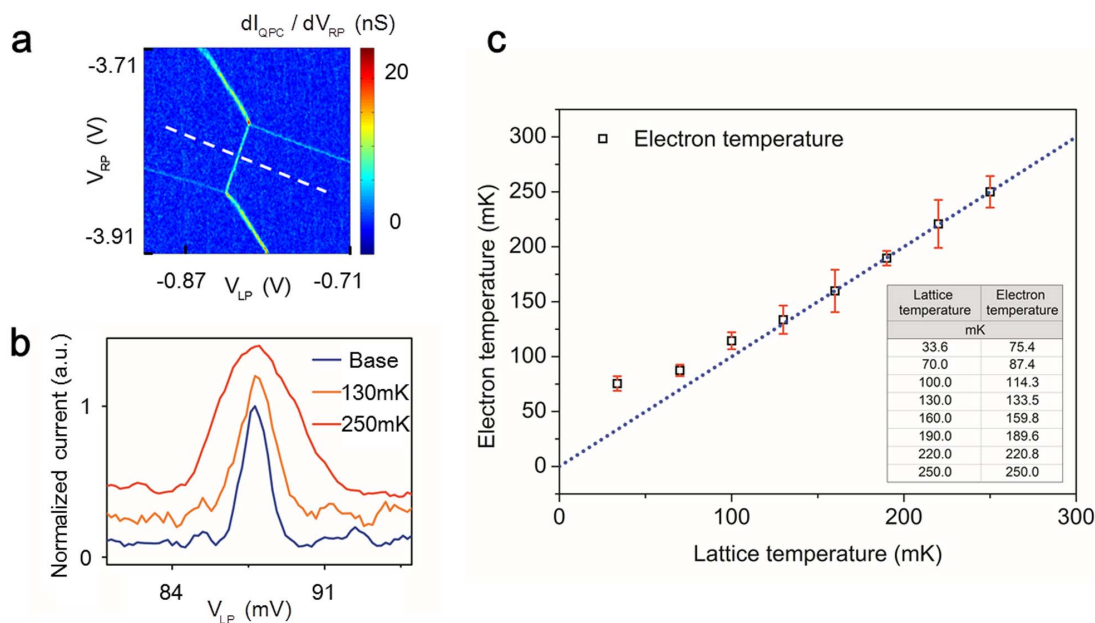

Figure 2 | Measurement of electron temperature under the base temperature of dilution refrigerator. (a). Charge stability diagram in a weakly coupled region. The white dashed line indicates the scanning direction for the transition peak broadening study, which is perpendicular to the transition line and is along the detuning direction. (b). The curves are taken at different temperatures showing the temperature broadening effect of the transition peak. Curves are first normalized and then offset 0.2 for clarity. (c). Electron temperature, deduced from the peak-width, as a function of the lattice temperature. Dotted line is the best fit of the linear regime and its intercept reveals information of the coupling strength, from which we assure that t_C here is no more than 2 μeV. Such calibration measures the electron temperature accurately and we eventually obtain that T_e to be 75.3 ± 9.4 mK at the base temperature of the mixing chamber.

$F = FWHM(eV)/4k_BT_e$. After F obtained, solving eq. (1) about Δ, eventually we can extract the absolute value of t_C by multiply Δ with $2k_BT_e$.

Starting from the region showed in Fig. 3a, we have extracted t_C for 13 inter-dot transition lines, marked by the number of electrons in the right dot from N + 8 to N − 5 (Transition N refers to the inter-dot transition from (M, N) to (M + 1, N − 1), as shown in Fig. 3a).

As shown in Fig. 3b, it is apparent that the t_C increases monotonically as electrons are added one by one into the right QD. The measured maximum value is 300 ueV (transition N + 8), which corresponds a tunneling frequency of about 70 GHz and is more than 4 times the value for the minimum (transition N). Such regularity over large number of charge configurations appears to against the common perception that in etched QD t_C is nearly uncontrollable. We speculate our device design of all-metal side gates may have improved the stability of the electrostatic environment to a level that is suitable for other coherent control experiments over a large space of gate voltages. It is important to mention that although regularity is demonstrated here over the entire plane, such monotonicity does not survive over very large range of charge configurations (Detailed discussion of sample characterization including more quantitative investigation of devices fabricated through our procedures can be found in supplementary material followed). As shown in the Fig. 3c, a non-monotonic change has been observed. The possible mechanism of this anomalous behavior is likely due to the charge impurities in the substrate or edge localized states in the graphene nano-ribbon itself and will be discussed later.

In addition, we have studied the tunability of using a single metal gate. Fig. 4 shows the results for two inter-dot transition lines,
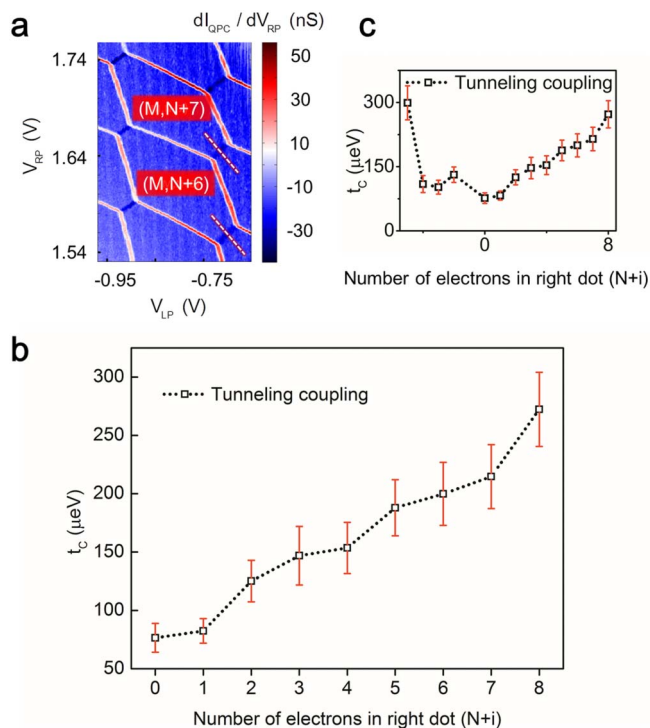
namely, transition N + 4 and N + 5. As we vary the voltage on the middle gate (MG), both curves change rapidly and saturated at large voltages. The t_C has been encouragingly changed by as much as a factor of 4 for a single gate. This voltage range is only about two units of charging energy Ec. The change of t_C can even be larger if we vary the voltages on other gates. Overall, with different gate combinations, we are able to vary the t_C from 2 ueV to 400 ueV. This tunability in gate voltage also encouragingly suggests that such devices can be an excellent platform for the fundamental research in this material that aims at demonstration of qubit operations. We would like to point out the controllable range of t_C in this work is well within the practical range for both coherent charge qubit[15,16] and spin qubit operations[17,18].

Discussion

Despite the encouraging facts that t_C can be well-tuned either by changing the number of electrons in a dot or by varying the voltage of a metallic gate, for a given charge configuration, anomalous behaviors are also observed.

As shown in Fig. 3c, while t_C decreases monotonically as the number of electrons is reduced from N + 8 to N, it increases from N − 1 to N − 5. The same thing happens when the tuning gate exceeds a certain voltage range, that is, when MG voltage is more negative than −150 mV ($\sim 1.5E_C$), the exponential increase suffers from a drop (not shown). We speculate that such anomalous behaviors are most-likely due to the edge-state-induced disorder, as they are shown to be inevitable in etched graphene ribbon structures[10–13]. The disorder can cause local electrochemical potential to fluctuate and form randomly distributed puddle states, that may or may not contribute to the DQD transport. The metallic gate can change the electrostatic potential smoothly in a short range. However, over large voltage range the capacitive coupling of the metallic gates to the puddle states can also add or subtract charges discretely to these parasitic dots, thus altered the entire environment abruptly and unexpectedly. Consequently, the DQD needs to re-configure itself leading to changes in both dot-gate capacitances and inter-dot tunneling strength. To describe this conjecture more intuitively, we use the schematic illustration in Fig. 5 as an example of a possible scenario. The DQD wavefunction in Fig. 5a is distorted as an electron is added discretely into one of the puddle states, as shown in Fig. 5b, which leads to an abrupt change in inter-dot coupling. More systematic investigation of the disorders in graphene nano-ribbons
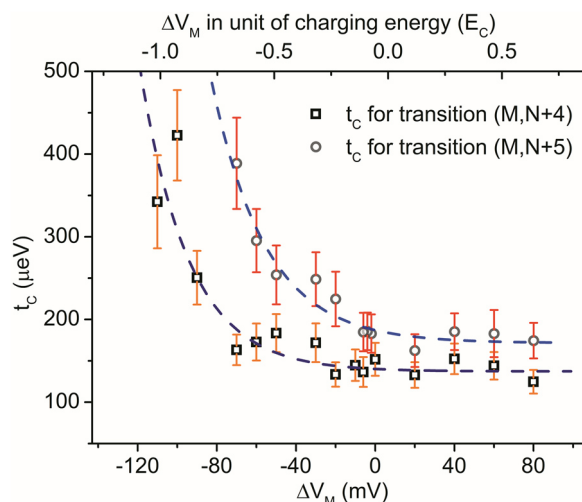

Figure 3 | Studying t_C's dependence on the relative electron number in one dot. (a). Region where we start to investigate t_C's dependence on electron number. Inter-dot tunnel coupling is measured along white dashed lines, which involve with different number of electrons in the dots, as shown. (b). t_C undergoes a monotonic increase from 70 μeV to 300 μeV as electron number increases. (c). When the measurement is extended over larger number of electrons, a non-monotonic change is observed. The anomalous behavior is interpreted as a result of disorder in the graphene nano-ribbons, as discussed in the text and in figure 5.

Figure 4 | Tuning t_C by middle gate. Inter-dot tunnel coupling as a function of the middle gate voltage. It shows that t_C can be modulated by about a factor of 4 by applying gate voltage on a single gate.
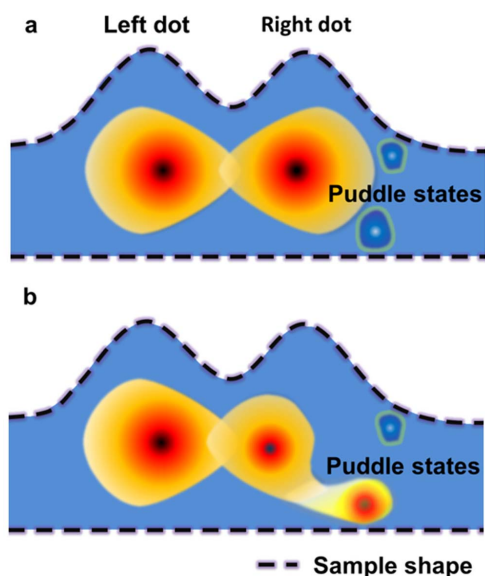
Figure 5 | Graphic illustration of an effect of puddle states on the inter-dot tunnel coupling. (a). The original states before b. (b). As an electron is added into the right dot, the DQD wavefunction is distorted leading to an abrupt change in inter-dot coupling.

may shed light on the microscopic details of the DQD re-configuration and thus is called for.

However, the effects of the imperfections should not impede the research progress in the etched graphene DQD structure, as our results encouragingly show that the gate control of t_C can be extended over a broad range of gate voltages and charge configurations. With steady improvement in the quality of graphene nano-ribbon, we fully expect the t_C tunability can eventually reach a level that is as good as that for DQDs made out of more conventional semiconductor, such as GaAs/AlGaAs[3] and Si/SiGe[4].

Last but not least, for graphene DQD to become a viable candidate for solid state qubits, not only controllable tunneling behavior of graphene nano-ribbon[19,20], but also suitable relaxation time (T_1)[20]/dephasing time (T_2) as well as coherent manipulation within such ranges should be demonstrated. Nevertheless, the study presented here suggesting sufficiently tunability of inter-dot coupling of graphene DQD may serve as a step forward in confirming such viability.

Methods

Device fabrication. The devices used for the experiment are fabricated as follow. We mechanically exfoliate graphene sheets from a KISH graphite and located them using prefabricated metal marks. We then use electron-beam lithography (EBL) to define the nano-ribbon structures of the DQD as well as the charge detection channel. The unwanted portion is then etched by Inductively Coupled Plasma (ICP) using a mixture of O2 and Ar (4 : 1). A second round of EBL is done using the precision alignment markers for placing Ti-Au (3 nm/20 nm) metal gates on top of the nano-ribbon structures. It is worth to note here, unlike the conventional fabrication techniques, we remove all the graphene materials other than the small DQD and QPC base structures. All the control gates are formed by metals instead of graphene to assure that gates are free of localized states.

Converting the detuning value from voltage to energy. Signal is obtained when sweeping LP and RP voltage along the white dashed line as shown in Fig. 2a and Fig. 3a, thus the preliminarily obtained FWHM of the transition peak is in unit of LP (or RP) gate voltage. For consistency we project such width to LP axis and denote such FWHM as FWHM (V). Further calculation asks for a conversion from voltage to energy (detuning), therefore we denote the converted FWHM as FWHM (eV).

These two values are related by a set of capacitances of the charge network[14]:

$$\text{FWHM(eV)} = \text{FWHM(V)} \cdot \left[\frac{C_{gL}(C_R - C_M)}{C_L C_R - C_M^2} \right] \cdot (1 + k^2) \qquad (3)$$

Here C_{gL} is the capacitance between left plunger gate and the left dot. C_L and C_R are the total capacitance of the left and right dot respectively. C_M is the interdot coupling

capacitance. Last but not least, k is the slope of the detuning line, as the dashed white line shown in Fig 2a.

Errors in the t_C determination. The error bars indicated in Fig. 3 and Fig. 4 can be categorized into three parts: 1) the uncertainty in measured base electron temperature ($\sim$8%), 2) error from the lever-arm for each inter-dot transition ($\sim$7%) and 3) measurement error of all the capacitances used to convert the FWHM from voltage to energy (3%). Altogether, those errors lead to an average uncertainty of 15%.

Admittedly, the amplitude of the modulation stimulus will induce a broadening effect ($\sim$5%) to the measured peak, when such amplitude exceeds 40% of the FWHM (V). However here in our measurements, we have minimized such effect by measuring each FWHM (V) under a set of different modulation amplitudes to make sure that we've reached the best signal-noise ratio and the least broadening effect at the same time.

1. Trauzettel, B., Bulaev, D. V., Loss, D. & Burkard, G. Spin qubits in graphene quantum dots. *Nature Phys.* **3**, 192–196 (2007).
2. Guo, G.-P., Lin, Z.-R., Li, X.-P., Tu, T. & Guo, G.-C. Quantum computation with graphene nanoribbon. *New J. Phys.* **11**, 123005 (2009).
3. DiCarlo, L. *et al*. Differential charge sensing and charge delocalization in a tunable double quantum dot. *Phys. Rev. Lett.* **92**, 226801 (2004).
4. Simmons, C. B. *et al*. Charge sensing and controllable tunnel coupling in a Si/SiGe double quantum dot. *Nano Lett.* **9**, 3234–8 (2009).
5. Wang, L. J. *et al*. Gates controlled parallel-coupled double quantum dot on both single layer and bilayer graphene. *Appl. Phys. Lett.* **99**, 112117 (2011).
6. Wang, L. J. *et al*. Controllable tunnel coupling and molecular states in a graphene double quantum dot. *Appl. Phys. Lett.* **100**, 022106 (2012).
7. Liu, X. L., Hug, D. & Vandersypen, L. M. K. Gate-defined graphene double quantum dot and excited state spectroscopy. *Nano Lett.* **10**, 1623–7 (2010).
8. Molitor, F. *et al*. Observation of excited states in a graphene double quantum dot. *Europhys. Lett.* **89**, 67005 (2010).
9. Connolly, M. R. *et al*. Gigahertz quantized charge pumping in graphene quantum dots. *Nature Nanotech.* **8**, 417–420 (2013).
10. Wang, L. J. *et al*. A graphene quantum dot with a single electron transistor as an integrated charge sensor. *Appl. Phys. Lett.* **97**, 262113 (2010).
11. Molitor, F. *et al*. Electronic properties of graphene nanostructures. *J. Phys. Condens. Matter* **23**, 243201 (2011).
12. Molitor, F. *et al*. Energy and transport gaps in etched graphene nanoribbons. *Semicond. Sci. Technol.* **25**, 034002 (2010).
13. Gallagher, P., Todd, K. & Goldhaber-Gordon, D. Disorder-induced gap behavior in graphene nanoribbons. *Phys. Rev. B* **81**, 115409 (2010).
14. Van Der Wiel, W. G. *et al*. Electron transport through double quantum dots. *Rev. Mod. Phys.* **75**, 1–22 (2003).
15. Petersson, K. D., Petta, J. R., Lu, H. & Gossard, A. C. Quantum coherence in a one-electron semiconductor charge qubit. *Phys. Rev. Lett.* **105**, 246804 (2010).
16. Cao, G. *et al*. Ultrafast universal quantum control of a quantum-dot charge qubit using Landau–Zener–Stückelberg interference. *Nature Commun.* **4**, 1401 (2013).
17. Petta, J. R. *et al*. Coherent manipulation of coupled electron spins in semiconductor quantum dots. *Science* **309**, 2180 (2005).
18. Maune, B. M. *et al*. Coherent singlet-triplet oscillations in a silicon-based double quantum dot. *Nature* **481**, 7381 (2012).
19. Güttinger, J. *et al*. Time-resolved charge detection in graphene quantum dots. *Phys. Rev. B* **83**, 165445 (2011).
20. Volk, C., Neumann, C. *et al*. Probing relaxation times in graphene quantum dots. *Nature Commun.* **4**, 1753 (2013).

Acknowledgments

Author contributions

D.W. fabricated the samples. D.W., G.L., Z.X.Z., H.O.L., G.C., M.X., G.P.G. and H.W.J. performed the measurements. D.W., T.T. and G.C.G. provided theoretical support. Data are analyzed by D.W., G.L. and Z.X.Z. The manuscript is prepared by D.W., H.W.J. and G.P.G., G.P.G. supervised the project. All authors contributed in discussing the results and commented on the manuscript.

Additional information

graphene double quantum dot by adjacent metal gates. *Sci. Rep.* **3**, 3175; DOI:10.1038/srep03175 (2013).